Hindawi
Advances in Polymer Technology
Volume 2020, Article ID 6438490, 12 pages
https://doi.org/10.1155/2020/6438490

Research Article

3-Bromopyridine-Heterogenized Phosphotungstic Acid for Efficient Trimerization of Biomass-Derived 5-Hydroxymethylfurfural with 2-Methylfuran to C_{21} Fuel Precursor

Yufei Xu, Zhaozhuo Yu, Hu Li, and Song Yang

State Key Laboratory Breeding Base of Green Pesticide & Agricultural Bioengineering, Key Laboratory of Green Pesticide & Agricultural Bioengineering, Ministry of Education, State-Local Joint Laboratory for Comprehensive Utilization of Biomass, Center for Research & Development of Fine Chemicals, Guizhou University, Guiyang, Guizhou 550025, China

Correspondence should be addressed to Hu Li; hli13@gzu.edu.cn and Song Yang; jhzx.msm@gmail.com

Received 8 August 2019; Revised 12 April 2020; Accepted 24 April 2020; Published 6 August 2020

Academic Editor: Leandro Gurgel

Copyright © 2020 Yufei Xu et al. This is an open access article distributed under the Creative Commons Attribution License, which permits unrestricted use, distribution, and reproduction in any medium, provided the original work is properly cited.

The production of long-chain carbon compounds (C_9-C_{21}) from biomass derivatives to alternate traditional fossil diesel is sustainable, eco-friendly, and potentially economic for modern industry. In this work, phosphotungstic acid heterogenized by 3-bromopyridine was achieved using a solvothermal method, which was demonstrated to be efficient for trimerization of biomass-derived 5-hydroxymethylfurfural (HMF) with 2-methylfuran (2-MF) to C_{21} fuel precursor (57.1% yield) under mild reaction conditions. The heterogeneous acidic catalyst could be reused for four consecutive cycles without obvious loss of activity, and different characterization techniques (e.g., XRD (X-ray diffraction), TG (thermogravimetric analysis), SEM (scanning electron microscope), FT-IR (Fourier transform infrared spectroscopy), and BET (Brunauer-Emmet-Teller)) were utilized to investigate the performance of the catalyst. In addition, a plausible reaction pathway was postulated, on the basis of results obtained by NMR (nuclear magnetic resonance) and GC-MS (gas chromatography-mass spectrometer). This strategy provides a facile and efficient approach to prepare a recyclable acidic catalyst for the production of diesel fuel precursor from biomass via controllable polymerization.

1. Introduction

To relieve the increasingly severe shortage issues of energy in modern society over the last decade, more and more new conversion systems are established to utilize or explore alternative energy (e.g., wind power, geothermal energy, tidal energy, and solar power) to replace traditional mineral fuels [1–5]. Unfortunately, fossil energy still takes a big part in our daily life especially automobile and jet fuels [6, 7]. Therefore, it is urgent to find a renewable and benign matter for energy production via a new type of synthetic approaches. The terrestrial biomass was regarded as an environmental and sustainable feedstock to produce various platform molecules which can be directly employed for the synthesis of biofuels or value-added chemicals [8–15].

Generally, the jet fuels are composed of long-chain carbon molecules that could be produced from oligomerization of low-carbon molecules via the C-C bond formation such as aldol condensation and alkylation in the presence of a basic or acidic catalyst [16–20]. In this regard, the environmental and energy problems could be addressed effectively by using biomass-derived long-chain carbon molecules to replace the petrochemical molecules as the fuel precursor. A C_{21} compound named 5-(bis(5-methylfuran-2-yl)methyl)-5′-methyl-2,2′-bifuran (MMBM), which is derived from condensation of biobased 2-methylfuran (2-MF) and 5-hydroxymethylfurfural (HMF) with an acid catalyst, is a cost-effective and promising biochemical for producing drop-in fuels [21] and can be directly employed to increase the fuel combustion efficiency. In addition, after hydrogenolysis, MMBM can be used as high-quality fuels (Scheme 1) [22],

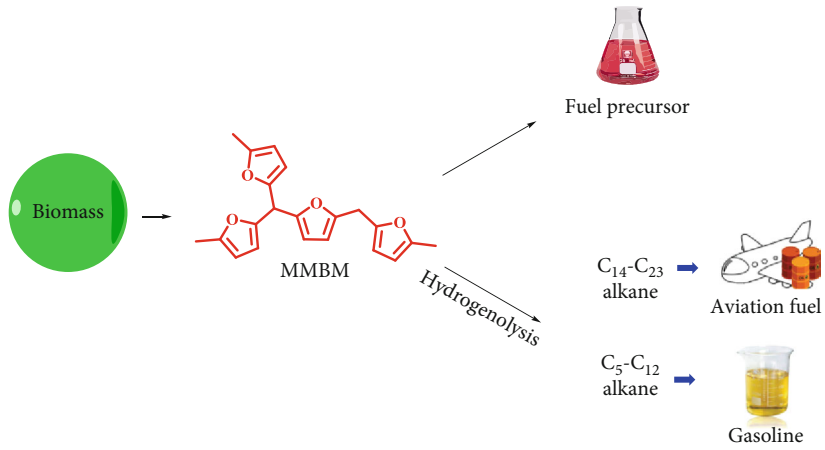

Scheme 1: The production and application of biomass-based C_{21} compound (MMBM).

such as aviation [23, 24] and diesel fuels [25]. Therefore, the production of such biomass-based C_n compounds for high-quality biofuels has attracted the researchers' interests in recent years.

In 2011, Corma et al. [24] utilized the 2-MF as the substrate to get the C_{15} fuel molecule precursor (5,5-bis(5-methylfuran-2-group)penta-2-ketone) using H_2SO_4 as an acid catalyst. A total yield of 87% C_n fuel molecule precursor could be achieved through the hydroxyalkylation/alkylation process. However, the shortcomings are also obvious; for example, (1) the acid catalyst H_2SO_4 is harmful to the environment, and (2) the homogenous catalyst would be lost and could not be reused after one reaction cycle. In 2017, Dutta et al. [25] came up with a modified graphene material to catalyze HMF and 2-MF into MMBM under 63°C for 12 h. In 2018, Wang et al. [26] and Gebresillase et al. [27] also prepared Sn-K-10 and KCC-IAPSO$_3$H as acidic catalysts for the condensation of 2-MF with acetic anhydride and 2-MF with furfural, *n*-butyraldehyde, or 2-pentanone into C_{17} or C_{14}-C_{15} fuel precursors under relatively mild conditions, respectively. These reaction systems can achieve the conversion of biomass platform molecules into long-chain molecule precursors by using acid catalysts, while the main disadvantage is that the catalyst preparation methods are too complicated and the cost is too high.

HPAs (heteropoly acids) with superb strong acidity are extensively used as economic and environmental catalysts in organic synthesis [28–32]. In particular, phosphotungstic acid (HPW, $H_3PW_{12}O_{40}$) has a tetrahedral PO_4 core in the center of the anion structure, surrounded by twelve WO_6 polyhedra via oxygen atoms to link each other, which exhibits excellent catalytic activity for upgrading biomass-derived compounds into different valuable chemicals and biofuels [33, 34]. However, it should be mentioned that HPW is extremely soluble into most polar solvents, difficult to separate, corrosive to reactors, and polluted to the environment [35–48]. Taking the above problems into consideration, it is highly desirable to heterogenize HPW using a high-efficiency method. For example, Wang et al. [50] and Fang et al. [51] prepared electric flocculation of HPW and silica-supported HPW heterogeneous catalysts for the conversion of glucose into 5-hydroxymethylfurfural (HMF) with a good yield of 61.7% and 78.3%, respectively. Due to heterogeneous functionalization, these catalysts could be reused at least four or five times without significant loss of catalytic activity. The incorporation of organic moieties (e.g., pyridine) is also illustrated to be capable of heterogenizing HPW, which was illustrated to be efficient for the conversion of HMF to 5-ethoxymethylfurfural (EMF) as well as fructose to ML with 90% and 82.5% yield, respectively. In view of the robust structure and good reactivity of the HPW-based acidic catalyst, it is highly promising to design novel solid acid by appropriate modification of HPW to match the desired biomass conversion processes.

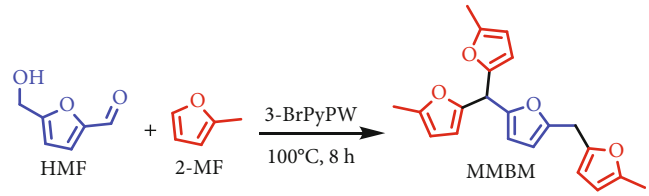

Scheme 2: The synthesis of C_{21} fuel precursor (MMBM) from the trimerization of HMF with 2-MF catalyzed by 3-BrPyPW.

In the present study, 3-bromopyridine was found to be effective for heterogenization of HPW, and the resulting acidic catalyst (3-BrPyPW) was active for the trimerization of biomass-derived HMF with 2-methylfuran (2-MF) to produce C_{21} fuel precursor (MMBM), as shown in Scheme 2. The reaction parameters and relevant mechanism were also investigated.

2. Experimental Section

2.1. Materials. 2-Methylfuran (2-MF, 99%), 5-hydroxymethyl-2-furaldehyde (HMF, 99%), dichloromethane (DCM, 99%), 1,4-dioxane (99%), naphthalene (99%), ethanol (99%), methanol (99%), phosphotungstic acid (HPW, 99.0%), 3-bromopyridine (3-BrPy) (98.0%), pyridine (Py, 98.0%), Amberlyst-15, and Nafion-117 were purchased from Beijing Innochem Technology Co., Ltd. 1,2-Dichloroethane was purchased from Sigma-Aldrich Co. LLC.

2.2. Catalyst Preparation. 3-BrPyPW was prepared by using a solvothermal method. Firstly, 1.1 mmol HPW and 30 mL ethanol were added into a 150 mL round-bottom flask with a magneton and stirred at 25°C to get a clear HPW solution; then, 1 mmol 3-BrPy was added into the solution with continuous stirring for 1.5 h at 25°C. The turbid liquid was poured into a 100 mL Teflon reactor, followed by transfer into a stainless steel autoclave. The sealed stainless steel autoclave was then placed in a muffle furnace set at 90°C for 12 h. Upon completion, precipitation could be obtained after filtration, and the resulting white solid was further washed with 20 mL ethanol for three times to ensure the redundant reactants be removed, and 3-BrPyPW was obtained after drying at 80°C overnight. The HPyPW catalyst was prepared using the same method for the preparation of 3-BrPyPW, in which the organic ligand pyridine was used instead of 3-BrPy under otherwise identical conditions.

2.3. Catalyst Characterization. The FT-IR spectra of the catalysts were recorded by a Fourier transform infrared spectrometer (Nicolet iS50) with KBr disk. An X-ray diffractometer (D8 Advance) with CuKα radiation ($\lambda = 0.1548$ nm) in the range of 5° to 80° was utilized to record the X-ray diffraction (XRD) patterns of catalysts. The SEM images and corresponding mapping images were obtained by a scanning electron microscope (FESEM XL-30; Philips). The TG curves were obtained by using a thermal gravimetric analyzer (STA409) with 10°C min^{-1} heating rate in an atmosphere of dry air. The N_2 adsorption-desorption experiment was carried out at -196°C using an ASAP 2460 equipment (Micromeritics). Firstly, the catalyst was outgassed for 12 h at 150°C. Then, the specific surface area was got by using the Brunauer-Emmett-Teller (BET) method, and the average pore size was obtained by using the Barrett-Joyner-Halenda (BJH) method. The XPS (X-ray photoelectron spectroscopy) data were collected by a Physical Electronics Quantum 2000 Scanning ESCA Microprobe (Physical Electronics Inc., PHI, MN) equipped with a monochromatic AlKα anode. ICP (inductively coupled plasma emission spectroscopy) analysis was conducted using a 5300 DV device (PerkinElmer Inc., Waltham, MA).

The total acid density of the catalyst was determined by the Na^+ exchange method. Firstly, 50 mg of solid catalyst was added to a sodium chloride solution (2 mol/L, 15 mL). The catalyst was oscillated by ultrasound for 0.5 h (2 mol/L, 5 mL/time), then washed three times, and the supernatant was collected by using a centrifuge, and the resulting supernatant was placed into a conical flask. Titrating the collected solution with sodium oxide solution (0.08213 mol/L), the solution with phenolphthalein will become red after the last drop of sodium hydroxide solution was added. It could be the endpoint of titration if the solution color remains for 30 seconds. The volume of consumed sodium hydroxide solution also needs to be recorded. The total acid density of the catalyst can be expressed as

$$C(H^+) = (V_{\mathrm{NaOH}} \times C_{\mathrm{NaOH}})/m. \quad (1)$$

$C(H^+)$ could be used as the total acid density (mol/g) of the catalyst, and m represents the mass (mg) of the catalyst. C_{NaOH} is the concentration of sodium hydroxide (mol/L). V_{NaOH} stands for the volume of consumed NaOH solution (L) during the titration.

2.4. Reaction Procedures for the Synthesis of MMBM from 2-MF and HMF. In a general reaction procedure, 3 mmol 2-MF and 1 mmol HMF, 20 mg 3-BrPyPW catalyst, 2 mL solvent (dichloromethane), and a magnetic bar were added into a 15 mL Ace pressure tube, which was then placed into an oil bath preheated to 100°C. After reaching the desired reaction time, the tube was taken out from the oil bath and cooled to room temperature with flowing tap water. Prior to quantitative analyses with GC (gas chromatography), the reaction solution was diluted with CH_2Cl_2 and filtered to remove solid catalyst with a filter membrane.

2.5. Product Analysis. An Agilent 7890B gas chromatography (GC) with an HP-5 column and FID detector was used to analyze the concentration of reactants and products, and 10 mg naphthalene was added as internal standard. An Agilent 6890N GC/5973 MS (GC-MS (gas chromatography-mass spectrometer)) was utilized to identify by-products. The conversion of 2-MF and yield of MMBM were obtained by using below calculation equations:

$$\begin{aligned} 2-\mathrm{MF\ conversion}\,(\%) &= \left[1 - \frac{\text{mole concentration of } 2-\mathrm{MF} \text{ in product}}{\text{mole concentration of initial } 2-\mathrm{MF}}\right] \times 100\%, \\ \mathrm{MMBM\ yield}\,(\%) &= \left[\frac{\text{mole concentration of MMBM}}{\text{mole concentration of initial } 2-\mathrm{MF}}\right] \times 100\%. \end{aligned} \quad (2)$$

2.6. Catalyst Recycling Study. After each cycle of the reaction, the catalyst was removed from the reaction system by centrifugation and then washed with 20 mL ethanol for three times, which was finally dried at 80°C for 24 h. The recovered catalyst was utilized directly for the next run under identical reaction conditions.

3. Results and Discussion

3.1. Catalyst Characterization. In order to understand the crystal structure of the prepared catalysts, the XRD patterns of 3-BrPyPW, HPyPW, and HPW were recorded and are shown in Figure 1. A Keggin anion cubic structure belonging

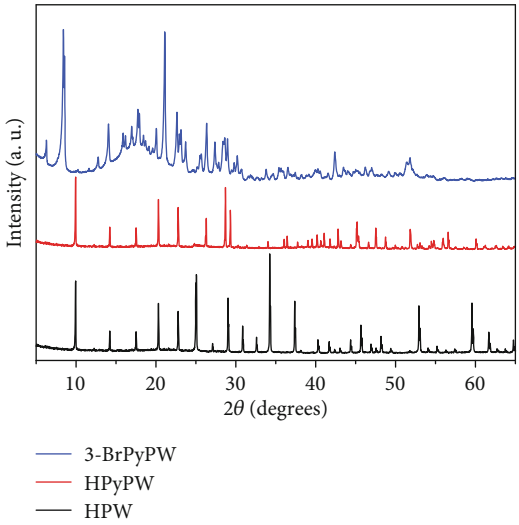

Figure 1: XRD patterns of 3-BrPyPW, HPyPW, and HPW.

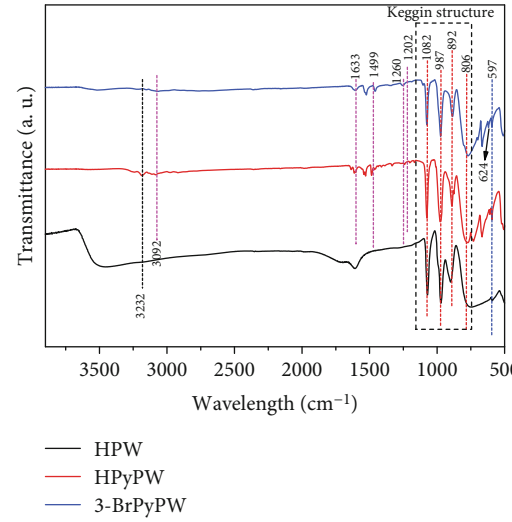

Figure 2: FT-IR spectra of 3-BrPyPW, HPyPW, and HPW.

to HPW with diffraction peaks at 9.9°, 14.1°, 17.6°, 20.3°, 22.7°, 24.8°, 29.1°, and 34.1° [50–56] could also be observed for HPyPW and 3-BrPyPW. This result indicated that even HPW was decorated by different organic species; it could well maintain the original HPW cubic basically. Moreover, due to the introduction of organic ligands, peaks in relatively low intensity appeared for both HPyPW and 3-BrPyPW, with the 2θ values having a negative shift to a lower angle. This phenomenon can be attributed to the electrostatic interaction between HPW and ligands [48, 49]. Moreover, some unknown diffraction peaks could be observed in 3-BrPyPW and HPyPW, and the possible explanation is that two catalysts will absorb some organic moieties, and this phenomenon has been proved by a previous work [51].

The FT-IR spectra of 3-BrPyPW, HPyPW, and HPW are shown in Figure 2. It could be clearly seen that specific peaks of a Keggin structure appear at the fingerprint region of 800 to 1100 cm^{-1} for each catalyst, and the characteristic peaks at 806 cm^{-1}, 892 cm^{-1}, 987 cm^{-1}, and 1082 cm^{-1} are attributed to asymmetric vibrations of the W-O_c, W-O_b, W-O_d, and P-O_a bonds, respectively, with a characteristic peak at 594 cm^{-1} being assigned to bending vibration of the P-O bond [48]. It means the presence of the characteristic structure of HPW in the as-prepared 3-BrPyPW and HPyPW catalysts, which agrees with the XRD results. In addition, the absorption peaks of pyridine structure were observed at 1633 cm^{-1} ($\nu_{C=C}$), 1499 cm^{-1} ($\nu_{C=N}$), 1262 cm^{-1} (δ_{C-H}), 1202 cm^{-1} (γ_{C-H}), and 3092 cm^{-1} (stretching vibration of benzene C-H bands) in both 3-BrPyPW and HPyPW catalysts, clearly indicating the existence of pyridine moieties.

The SEM image was used to investigate the morphology of 3-BrPyPW and is shown in Figure 3. It could be seen that the 3-BrPyPW displayed a polyhedral block structure, which closely agrees with the XRD results (Figure 1). In addition, when the N, O, P, W, and Br elemental mappings of 3-BrPyPW were analyzed (Figure 3), it was found that each element is well dispersed on the catalyst surface. This also laterally proved the successful preparation of 3-BrPyPW. This result was further confirmed by XPS and ICP analysis. For 3-BrPyPW, 65 wt% of W species and 4 wt% of P species could be detected by ICP analysis, while 5 wt% of C and 2 wt% of N could be attained by XPS analysis. On the other hand, 69 wt% of W species and 3 wt% of P species could be detected by ICP analysis, while 3 wt% of C and 1 wt% of N could be obtained by XPS analysis in the HPyPW sample. These results show that almost equivalent HPW and ligands are connected to each other through electrostatic interaction.

The N_2 adsorption-desorption isotherms of the 3-BrPyPW, HPyPW, and HPW are shown in Figure 4. Three typical H_4-type adsorption-desorption isotherm curves could be observed. For the catalyst BET specific surface area, it can be arranged in the following order: 3-BrPyPW (120.5 m^2/g)>HPyPW (115.4 m^2/g)>HPW (4.8 m^2/g), with the arrangement of BJH average pore size as follows: 3-BrPyPW (13.5 nm)>HPyPW (5.6 nm)>HPW (3.5 nm). Moreover, the total acid density of three catalysts was also tested. It could be found that 3-BrPyPW has a relatively high acid density (2.54 mmol/g) compared to HPyPW (0.51 mmol/g) and HPW (1.54 mmol/g) (Table 1). Therefore, in comparison with HPyPW and HPW, a higher specific surface area, larger pore size, and higher total acid density may make 3-BrPyPW have a superior activity in the conversion of 2-MF and HMF to MMBM.

3.2. Catalyst Screening for the Conversion of 2-MF and HMF to MMBM. The synthesis of MMBM from HMF and 2-MF in CH_2Cl_2 under 100°C for 8 h was investigated in the presence of different catalysts, and the obtained results are shown in Table 2. HPW gave 81.7% 2-MF conversion and 32.9% MMBM yield. After being functionalized with pyridine, it was found that the resulting HPyPW catalyst showed poor reactivity with 21.1% 2-MF conversion while just 0.1% MMBM yield. To our surprise, 3-BrPyPW exhibited a superior catalytic performance with 82.0% 2-MF conversion and 57.1% MMBM yield. The introduction of the electronegative substituent was proposed to cause an inductive effect and steric hindrance, which might improve the catalyst structure, thus affording enhanced catalytic activity [49]. Amberlyst-

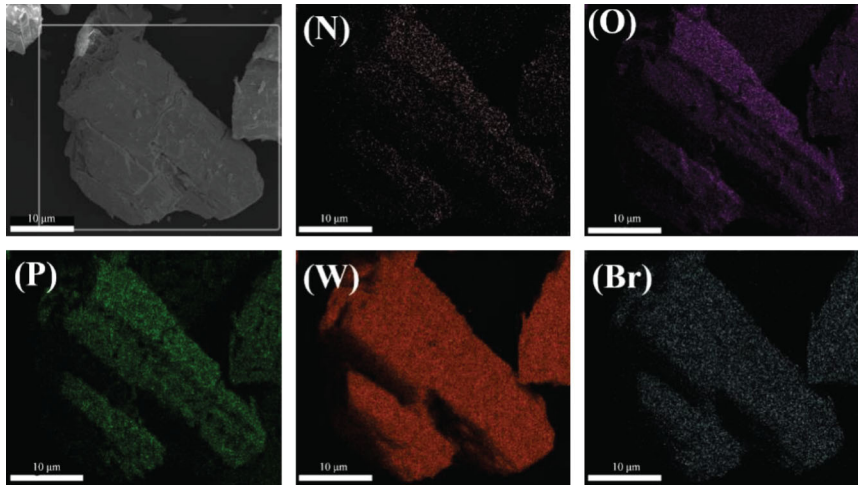

Figure 3: SEM image and elemental mappings of the 3-BrPyPW catalyst.

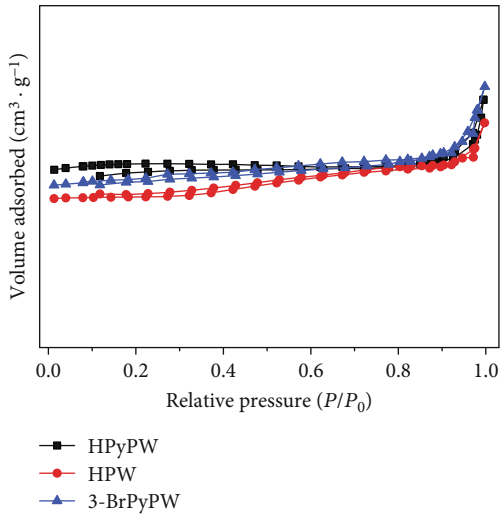

Figure 4: The N_2 adsorption-desorption isotherms of 3-BrPyPW, HPyPW, and HPW.

Table 1: Acid density, pore size, and specific surface area comparison of 3-BrPyPW, HPyPW, and HPW.

Catalyst	Acid density (mmol/g)	Average pore size (nm)	S_{BET} (m^2/g)
3-BrPyPW	2.54	13.5	120.5
HPyPW	0.51	5.6	115.4
HPW	1.54	3.5	4.8

15 and Nafion-117 were also investigated for comparison, and 37.9% and 76.4% 2-MF conversion with 12.3% and 25.8% MMBM yield could be achieved, respectively. These experimental results are consistent with those of previous reports, with respect to the BET specific surface area, average pore size, and total acid density. By introducing the 3-BrPy ligand, the obtained 3-BrPyPW catalyst has a larger specific surface area and pore size, so that it can get a better reaction activity compared to HPyPW and HPW. Furthermore, a good acid density may also contribute to the pronounced yield of MMBM. Therefore, 3-BrPyPW is a better catalyst for the investigated reaction, which was thus selected for further optimization.

Table 2: Catalytic results for the synthesis of MMBM from 2-MF and HMF over different catalysts.

Catalyst	Yield (MMBM, %)	Conversion (2-MF, %)
HPW	32.9	81.7
HPyPW	0.1	21.1
3-BrPyPW	57.1	82.0
Amberlyst-15	12.3	37.9
Nafion-117	25.8	76.4

Reaction conditions: 3 mmol 2-MF, 1 mmol HMF, 20 mg catalyst, 2 mL solvent, 100°C, and 8 h.

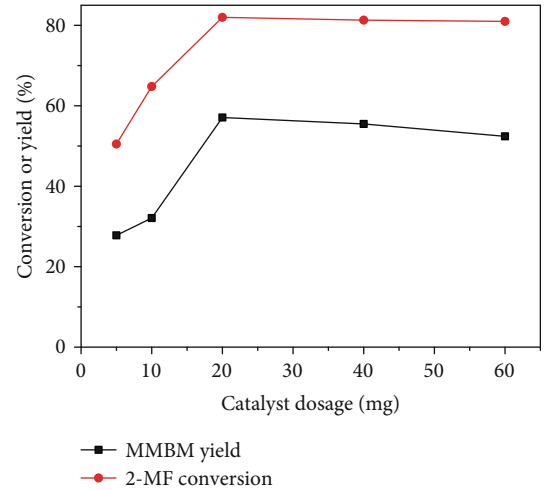

Figure 5: The influence of the 3-BrPyPW catalyst dosage on the synthesis of MMBM from HMF and 2-MF. Reaction conditions: 3 mmol 2-MF, 1 mmol HMF, 2 mL CH_2Cl_2, 100°C, and 8 h.

3.3. The Effect of the Catalyst Dosage on the Synthesis of MMBM from HMF and 2-MF. The impact of the 3-

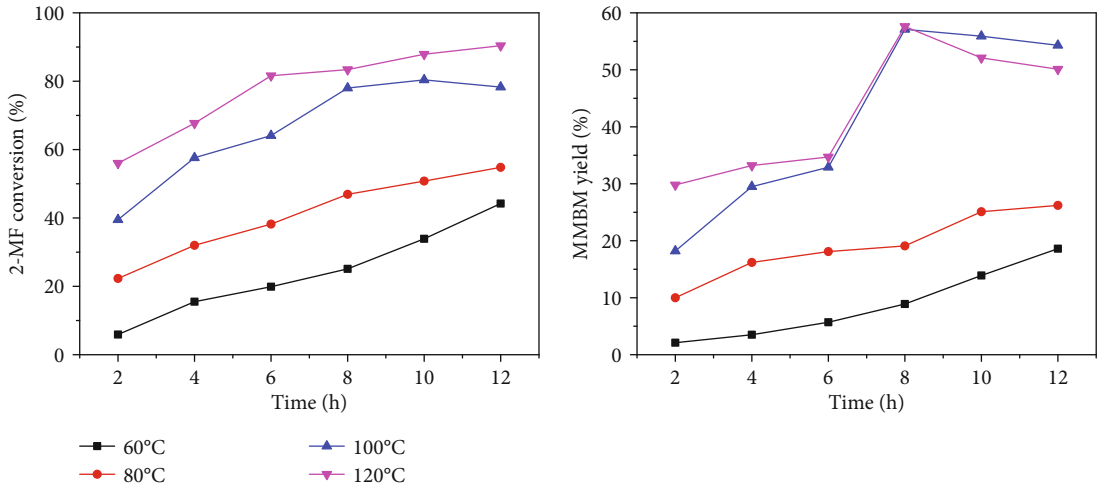

Figure 6: Influence of reaction temperature/time on the conversion of HMF and 2-MF to MMBM. Reaction conditions: 3 mmol 2-MF, 1 mmol HMF, 20 mg 3-BrPyPW, and 2 mL CH_2Cl_2.

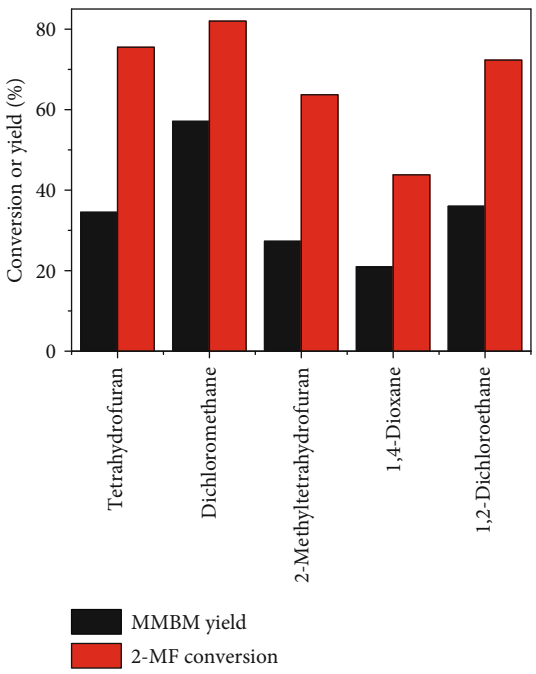

Figure 7: The influence of the solvent type on the synthesis of MMBM from HMF and 2-MF. Reaction conditions: 3 mmol 2-MF, 1 mmol HMF, 2 mL solvent, 100°C, and 8 h.

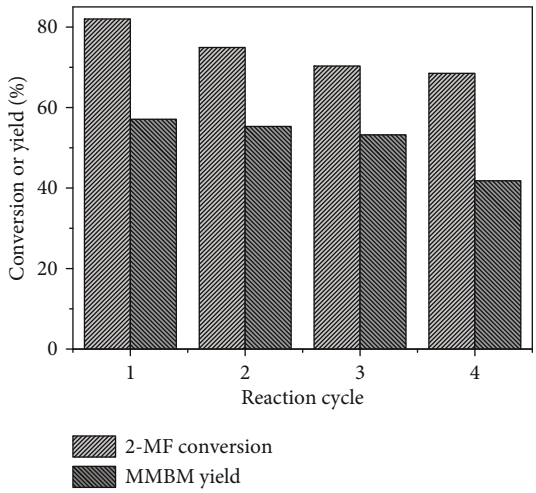

Figure 8: The 3-BrPyPW catalyst recycling study. Reaction conditions: 3 mmol 2-MF, 1 mmol HMF, 20 mg 3-BrPyPW, 2 mL CH_2Cl_2, 100°C, and 8 h.

BrPyPW catalyst dose on the conversion of HMF and 2-MF to MMBM was examined (Figure 5). The conversion of 2-MF and yield of MMBM increased from 50.5% to 82.0% and 27.8% to 57.1% with the increase of the catalyst dosage from 5 mg to 20 mg. When a higher amount of catalyst of 40 mg and 60 mg was employed for the reaction, the yield of MMBM decreased to 55.5% and 52.4%, respectively, but no obvious change in 2-MF conversion was observed. This result may be due to the occurrence of side reactions using a relatively higher catalyst dosage. The possible reason is that the substrate HMF would be converted to by-products, such as maleic acid, as determined by NMR spectra (Figure S1), which is in good agreement with previous works [55, 56]. Therefore, 20 mg 3-BrPyPW was chosen as the best catalyst dosage for the trimerization reaction.

3.4. Influence of Reaction Temperature/Time on the Synthesis of MMBM from HMF and 2-MF. The reaction temperature and time were found to be important for the synthesis of MMBM from HMF and 2-MF. A range of reaction temperatures (60, 80, 100, and 120°C) with varying reaction time from 2 to 12 h was utilized to optimize the reaction conditions (Figure 6). It could be found that with increasing the reaction temperature and time, the conversion of either 2-MF or HMF gradually increased, and a maximum 2-MF conversion of 90.4% was obtained at 120°C for 12 h. The yield of MMBM kept increasing with raising the temperature from 60 to 120°C reacting for 2 to 8 h, where 57.1% and 57.6% yield of MMBM could be achieved at 100 and 120°C for 8 h,

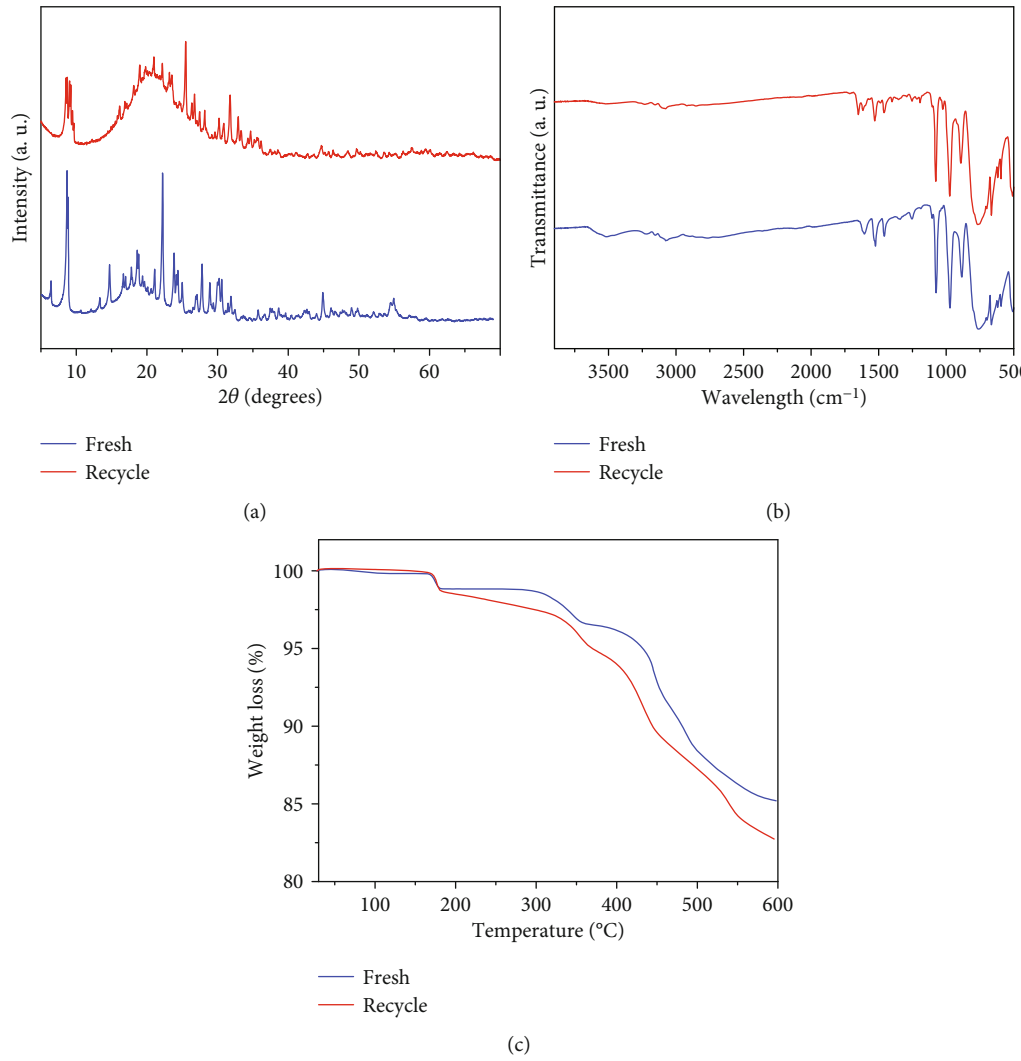

Figure 9: XRD patterns (a), FT-IR spectra (b), and TGA curves (c) of the recycled (after the fourth run) and fresh 3-BrPyPW catalysts.

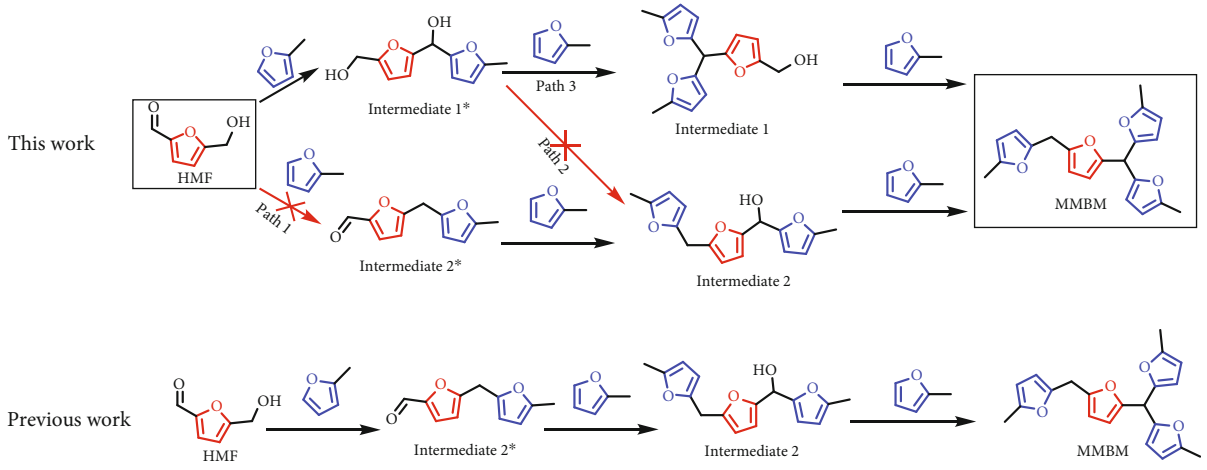

Scheme 3: Comparison of reaction pathways for the conversion of HMF and 2-MF to MMBM in this work and reported work.

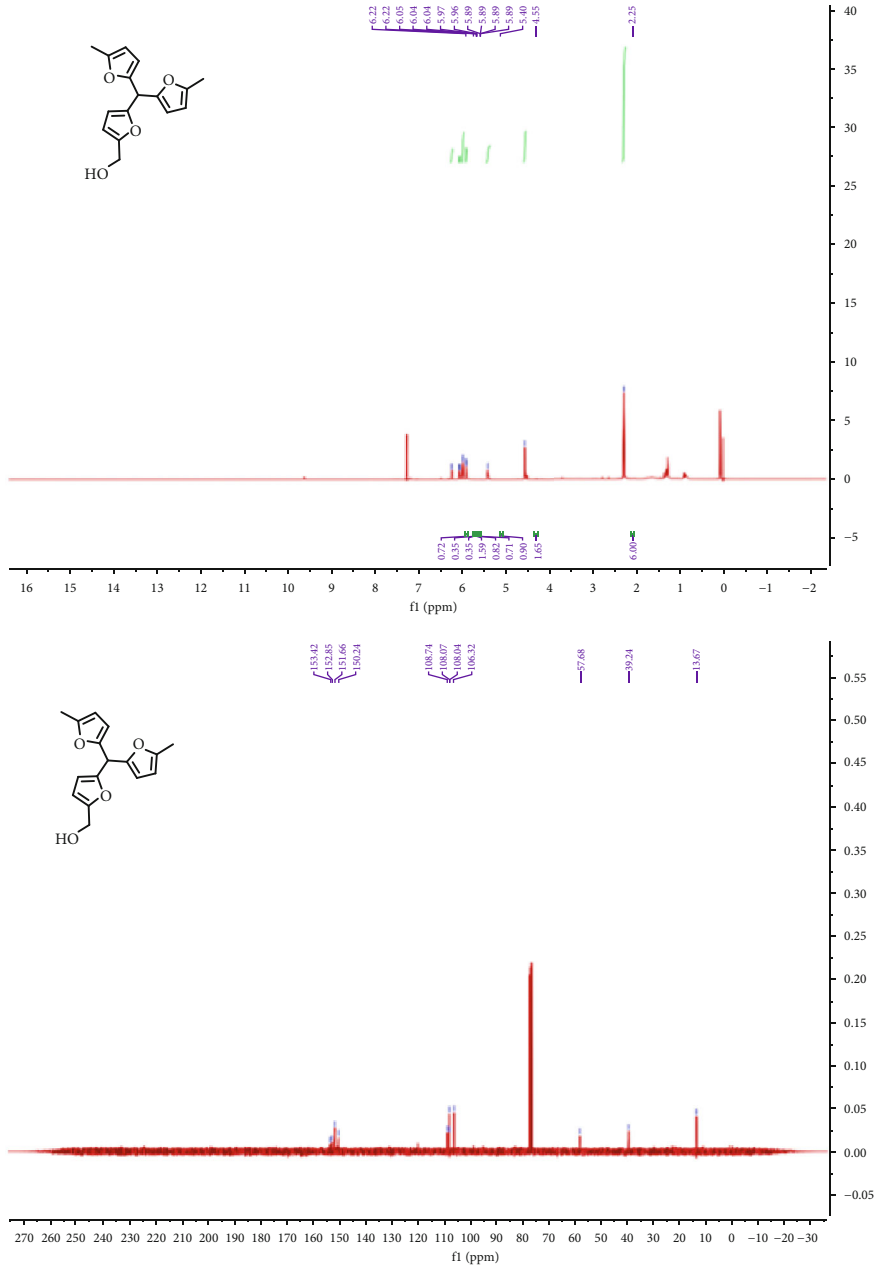

Figure 10: ^{1}H and ^{13}C NMR spectra of intermediate 1. Intermediate 1: ^{1}H NMR (500 MHz, $CDCl_3$) δ = 6.22 (*d*, *J* = 3.2 Hz, 1H), 6.05 (s, 1H), 6.04 (*d*, *J* = 0.7 Hz, 1H), 5.97 (*d*, *J* = 3.1 Hz, 2H), 5.89 (*d*, *J* = 1.0 Hz, 1H), 5.89 (*d*, *J* = 1.0 Hz, 1H), 5.40 (s, 1H), 4.55 (s, 2H), 2.25 (s, 6H). ^{13}C NMR (126 MHz, $CDCl_3$) δ = 153.42, 152.85, 151.66, 150.24, 108.74, 108.05, 106.32, 57.68, 39.24, 13.67.

respectively. However, when the reaction time continued to increase from 8 to 12 h, a decline in MMBM yield from 57.1% and 57.6% to 54.3% and 50.1% was detected at 100°C and 120°C, respectively. It was indicated that the extension of reaction time led to a decrease of MMBM yield, which may be due to the happening of side reactions. For example, HMF would be transformed into by-products, like oxidation to maleic acid, as determined by NMR spectra (Figure S1) for long reaction time with an excess amount of the 3-BrPyPW catalyst [55, 56]. So, a higher temperature led to the increase of substrate conversion but with no significant contribution to raising the yield of MMBM. On account of saving energy consumption, 100°C and 8 h were chosen as the optimum reaction temperature and time, respectively.

3.5. The Effect of the Solvent Type on the Synthesis of MMBM from HMF and 2-MF. The reaction solvent also has a great influence on the synthesis of MMBM from HMF and 2-MF. Figure 7 shows the corresponding screening results of different reaction solvents (tetrahydrofuran, dichloromethane, 2-methyltetrahydrofuran, 1,4-dioxane, and 1,2-dichloroethane). As tetrahydrofuran and dichloromethane were used as solvent, 34.5% and 57.1% yield of MMBM with

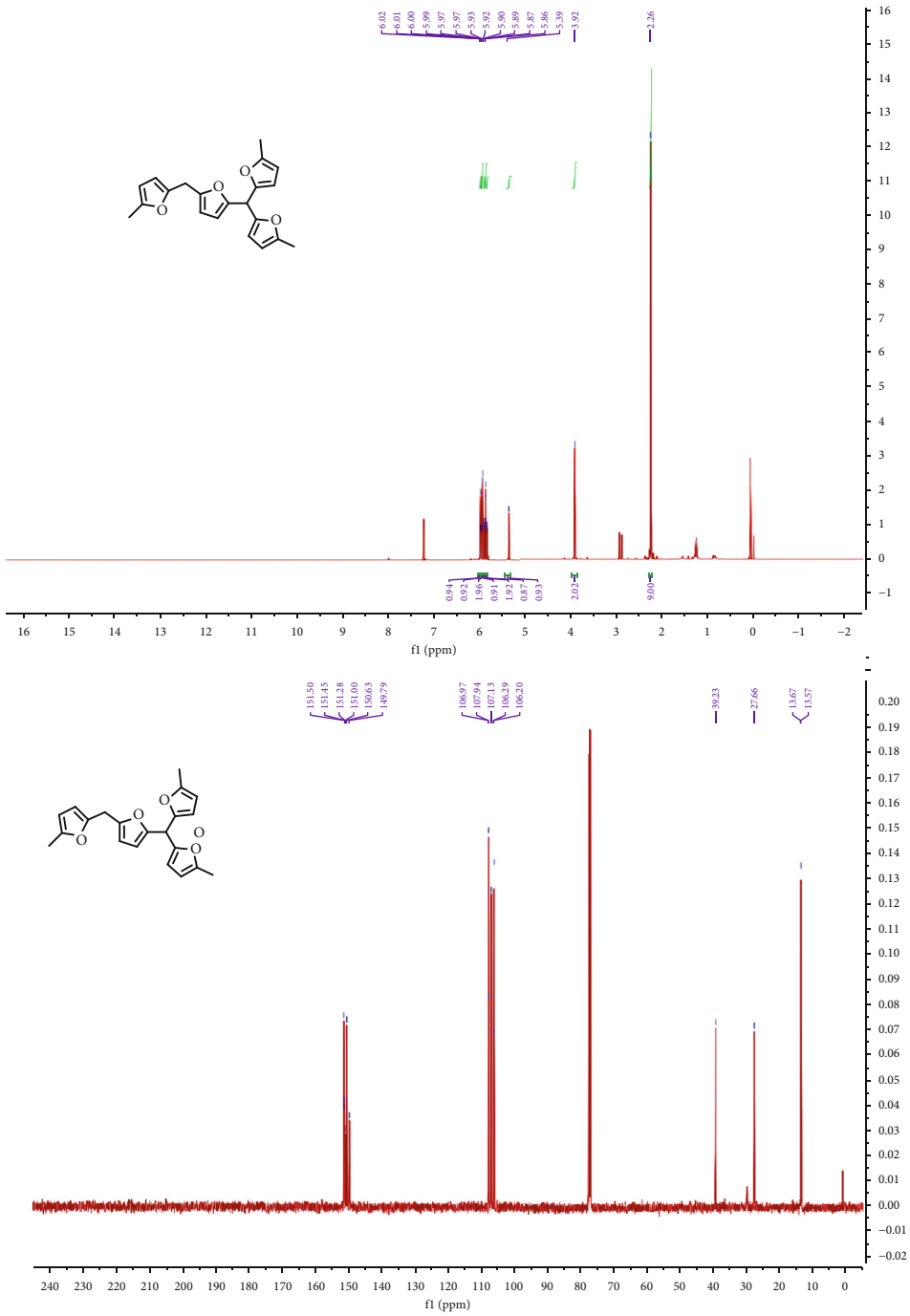

Figure 11: ^{1}H and ^{13}C NMR spectra of MMBM. MMBM: ^{1}H NMR (500 MHz, $CDCl_3$) δ = 6.01 (*d*, *J* = 3.7 Hz, 1H), 6.00 (*d*, *J* = 3.2 Hz, 1H), 5.97 (*d*, *J* = 3.1 Hz, 2H), 5.93 (*d*, *J* = 3.0 Hz, 1H), 5.90 (*d*, *J* = 3.1 Hz, 2H), 5.87 (*d*, *J* = 2.9 Hz, 1H), 5.39 (s, 1H), 3.92 (s, 2H), 2.26 (s, 9H). ^{13}C NMR (126 MHz, $CDCl_3$) δ = 151.50, 151.45, 151.28, 151.00, 150.63, 149.79, 107.97, 107.94, 107.13, 106.29, 106.20, 39.23, 27.66, 13.67, 13.57.

75.5% and 82.0% 2-MF conversion can be achieved, respectively. When 2-methyltetrahydrofuran, 1,4-dioxane, and 1, 2-dichloroethane were employed, the yield of MMBM is 27.3%, 21.0%, and 36.0% which can be attained under the same reaction conditions, respectively. It is proposed that CH_2Cl_2 may act as an extractant to separate the target product MMBM from the in situ formed water in the reaction system, thus hindering its further degradation. According to this solvent screening experiment, dichloromethane was chosen as the best solvent for the reaction system.

3.6. Catalyst Recycling Study. The recyclability of 3-BrPyPW was tested in the synthesis of MMBM from HMF and 2-MF under optimum reaction conditions. Figure 8 shows that the MMBM yield decreased gradually from 57.1% to 41.8% while 2-MF conversion decreased from 82.0% to 68.5% after

four consecutive cycles, showing that the 3-BrPyPW catalyst is relatively stable for the trimerization reaction. Figure 9 collects the XRD patterns (Figure 9(a)), FT-IR spectra (Figure 9(b)), and TGA curves (Figure 9(c)) of the fresh and recycled 3-BrPyPW catalysts. For XRD patterns, it is not difficult to see that the intensity of fresh 3-BrPyPW was higher than that of the recycled counterpart, indicating that organic residues might be absorbed into the catalyst after four reaction cycles [56]. Moreover, the ICP analysis of reused 3-Br-PyPW shows that there has no leaching of W species. Compared to fresh 3-BrPyPW, the FT-IR spectrum of the reused catalyst showed a relatively lower transmittance, which is a good agreement with the results obtained from XRD patterns. The TG curves of fresh and recycled 3-BrPyPW revealed that organic species might adhere to the catalyst after four consecutive reactions, which can be well supported by the result that recycled 3-BrPyPW has a drastic decline in weight loss compared to the fresh counterpart. This further indicated that the deposition of organic moieties is most likely to be the major factor that caused the loss of the catalyst activity. From above experiments, by comparing with previous studies [25, 57], 3-BrPyPW was demonstrated to show superior reactivity and stability in the production of MMBM from HMF and 2-MF under the examined reaction conditions in our work.

3.7. Reaction Mechanism Study. In order to investigate the reaction pathways for the trimerization of HMF with 2-MF to MMBM, the reaction mixture was recorded by GC-MS and NMR. Based on the experimental results, the possible reaction pathways were proposed and are shown in Scheme 3. The proposed reaction path was also compared with that of previous work reported by Dutta et al. [25] and Shinde et al. [57]. As identified by GC/MS, a compound with a molecular weight of 272.1 was formed during the reaction process. It is preliminarily assumed that its structure is intermediate 1, which was further confirmed by ^{1}H and ^{13}C NMR (Figure 10). On the other hand, MMBM was also detected by GC-MS (molecular weight 336.2) and confirmed by ^{1}H and ^{13}C NMR (Figure 11). This result revealed that intermediate 1∗ was formed from HMF and 2-MF, which further rapidly converted intermediate 1 and subsequently afforded the fuel precursor MMBM. However, both intermediates 2∗ and 2 were not detected by GC-MS, implying the reaction pathway might be neither path 1 nor path 2, and path 3 was most likely the dominant reaction pathway.

4. Conclusion

In summary, a halogenated pyridine-heterogenized HPW was prepared by a simple solvothermal method and used as a heterogeneous acidic catalyst for the conversion of HMF and 2-MF to MMBM. Single-factor optimization was utilized to test the catalytic performance of 3-BrPyPW; a good MMBM yield of 57.1% with 82.0% 2-MF conversion could be obtained under optimum reaction conditions (1 mmol HMF and 3 mmol 2-MF at 100°C for 8 h in 2 mL CH_2Cl_2). The 3-BrPyPW catalyst could be reused for four cycles without significant decreasing of its activity, which was characterized without obvious structure change after recycles. Moreover, a dominant reaction pathway for the synthesis of MMBM from HMF and 2-MF was elucidated.

Data Availability

The data used to support the findings of this study are included in the article.

Conflicts of Interest

There are no conflicts of interest regarding the publication of this paper.

Acknowledgments

This work was financially supported by the National Natural Science Foundation of China (21666008, 21576059, and 21908033), Fok Ying-Tong Education Foundation (161030), Key Technologies Research and Development Program of China (2014BAD23B01), and Guizhou Science & Technology Foundation ((2018)1037).

Supplementary Materials

Figure S1: ^{1}H and ^{13}C NMR spectra of maleic acid. *(Supplementary materials)*

References

[1] Y. Román-Leshkov, C. J. Barrett, Z. Y. Liu, and J. A. Dumesic, "Production of dimethylfuran for liquid fuels from biomass-derived carbohydrates," *Nature*, vol. 447, no. 7147, pp. 982–985, 2007.

[2] L. Zhang, B. Zhang, J. Chen et al., "Lawn structured triboelectric nanogenerators for scavenging sweeping wind energy on rooftops," *Advanced Materials*, vol. 28, no. 8, pp. 1650–1656, 2016.

[3] J. Unternährer, S. Moret, S. Joost, and F. Maréchal, "Spatial clustering for district heating integration in urban energy systems: application to geothermal energy," *Applied Energy*, vol. 190, pp. 749–763, 2017.

[4] E. Segura, R. Morales, and J. A. Somolinos, "A strategic analysis of tidal current energy conversion systems in the European Union," *Applied Energy*, vol. 212, pp. 527–551, 2018.

[5] Y. Yang, R. Zhao, T. Zhang et al., "Graphene-based standalone solar energy converter for water desalination and purification," *ACS Nano*, vol. 12, no. 1, pp. 829–835, 2018.

[6] M. Ross, "Automobile fuel consumption and emissions: effects of vehicle and driving characteristics," *Annual Review of Energy and the Environment*, vol. 19, no. 1, pp. 75–112, 1994.

[7] J. I. Hileman and R. W. Stratton, "Alternative jet fuel feasibility," *Transport Policy*, vol. 34, pp. 52–62, 2014.

[8] H. Li, A. Riisager, S. Saravanamurugan et al., "Carbon-increasing catalytic strategies for upgrading biomass into energy-intensive fuels and chemicals," *ACS Catalysis*, vol. 8, no. 1, pp. 148–187, 2017.

[9] F. D. Pileidis and M. M. Titirici, "Levulinic acid biorefineries: new challenges for efficient utilization of biomass," *ChemSusChem*, vol. 9, no. 6, pp. 562–582, 2016.

[10] A. Bohre, B. Saha, and M. M. Abu-Omar, "Catalytic upgrading of 5-hydroxymethylfurfural to drop-in biofuels by solid base and bifunctional metal-acid catalysts," *ChemSusChem*, vol. 8, no. 23, pp. 4022–4029, 2015.

[11] Y. Xu, J. Long, W. Zhao, H. Li, and S. Yang, "Efficient transfer hydrogenation of nitro compounds to amines enabled by mesoporous N-stabilized Co-Zn/C," *Frontiers in Chemistry*, vol. 7, p. 590, 2019.

[12] S. Shinde, K. Deval, R. Chikate, and C. Rode, "Cascade synthesis of 5-(acetoxymethyl)furfural from carbohydrates over Sn-Mont catalyst," *ChemistrySelect*, vol. 3, no. 30, pp. 8770–8778, 2018.

[13] N. Luo, T. Montini, J. Zhang et al., "Visible-light-driven coproduction of diesel precursors and hydrogen from lignocellulose-derived methylfurans," *Nature Energy*, vol. 4, no. 7, pp. 575–584, 2019.

[14] Y. Xu, J. Long, J. He, and H. Li, "Alcohol-mediated reduction of biomass-derived furanic aldehydes via catalytic hydrogen transfer," *Current Organic Chemistry*, vol. 23, no. 20, pp. 2168–2179, 2019.

[15] S. H. Shinde and C. V. Rode, "A two-phase system for the clean and high yield synthesis of furylmethane derivatives over -SO_3H functionalized ionic liquids," *Green Chemistry*, vol. 19, no. 20, pp. 4804–4810, 2017.

[16] R. Tripathi, U. Burke, A. K. Ramalingam et al., "Oxidation of 2-methylfuran and 2-methylfuran/n-heptane blends: an experimental and modeling study," *Combustion and Flame*, vol. 196, pp. 54–70, 2018.

[17] I. Gandarias, S. García-Fernández, I. Obregón, I. Agirrezabal-Telleria, and P. L. Arias, "Production of 2-methylfuran from biomass through an integrated biorefinery approach," *Fuel Processing Technology*, vol. 178, pp. 336–343, 2018.

[18] K. Alexandrino, C. Baena, Á. Millera, R. Bilbao, and M. U. Alzueta, "2-Methylfuran pyrolysis: gas-phase modelling and soot formation," *Combustion and Flame*, vol. 188, pp. 376–387, 2018.

[19] B. Wang, Z. Wang, X. Bao et al., "Microscopic investigation of near-field spray characteristics of 2-methylfuran, ethanol and isooctane under flash boiling conditions," *Fuel*, vol. 215, pp. 142–152, 2018.

[20] J. Xie, X. Zhang, Y. Liu et al., "Synthesis of high-density liquid fuel _via_ Diels-Alder reaction of dicyclopentadiene and lignocellulose-derived 2-methylfuran," *Catalysis Today*, vol. 319, pp. 139–144, 2019.

[21] H. Li, S. Saravanamurugan, S. Yang, and A. Riisager, "Catalytic alkylation of 2-methylfuran with formalin using supported acidic ionic liquids," *ACS Sustainable Chemistry & Engineering*, vol. 3, no. 12, pp. 3274–3280, 2015.

[22] D. Jin, C. Fang, Y. Li et al., "Catalytic dimerization of bio-based 5-methylfurfuryl alcohol to bis(5-methylfuran-2-yl) methane with a solid acidic nanohybrid," *Current Nanoscience*, vol. 16, no. 2, pp. 235–245, 2020.

[23] H. Li, Z. Gui, S. Yang, Z. Qi, S. Saravanamurugan, and A. Riisager, "Catalytic tandem reaction for the production of jet and diesel fuel range alkanes," *Energy Technology*, vol. 6, no. 6, pp. 1060–1066, 2018.

[24] A. Corma, O. de la Torre, M. Renz, and N. Villandier, "Production of high-quality diesel from biomass waste products," *Angewandte Chemie. International Edition*, vol. 123, no. 10, pp. 2423–2426, 2011.

[25] S. Dutta, A. Bohre, W. Zheng et al., "Solventless C-C coupling of low carbon furanics to high carbon fuel precursors using an improved graphene oxide carbocatalyst," *ACS Catalysis*, vol. 7, no. 6, pp. 3905–3915, 2017.

[26] Z. Wang, H. Li, W. Zhao, and S. Yang, "Low-temperature and solvent-free production of biomass-derived diesel-range C_{17} precursor via one-pot cascade acylation-alkylation over Sn^{4+}-montmorillonite," *Journal of Industrial and Engineering Chemistry*, vol. 66, pp. 325–332, 2018.

[27] M. N. Gebresillase, R. Shavi, and J. G. Seo, "A comprehensive investigation of the condensation of furanic platform molecules to C14–C15fuel precursors over sulfonic acid functionalized silica supports," *Green Chemistry*, vol. 20, no. 22, pp. 5133–5146, 2018.

[28] I. Weber, P. Friese, and M. Olzmann, "H-atom-forming reaction pathways in the pyrolysis of furan, 2-methylfuran, and 2, 5-dimethylfuran: a shock-tube and modeling study," *The Journal of Physical Chemistry. A*, vol. 122, no. 32, pp. 6500–6508, 2018.

[29] A. R. K. Gollakota, N. Kishore, and S. Gu, "A review on hydrothermal liquefaction of biomass," *Renewable and Sustainable Energy Reviews*, vol. 81, pp. 1378–1392, 2018.

[30] V. Heck, D. Gerten, W. Lucht, and A. Popp, "Biomass-based negative emissions difficult to reconcile with planetary boundaries," *Nature Climate Change*, vol. 8, no. 2, pp. 151–155, 2018.

[31] M. Borghei, J. Lehtonen, L. Liu, and O. J. Rojas, "Advanced biomass-derived electrocatalysts for the oxygen reduction reaction," *Advanced Materials*, vol. 30, no. 24, p. 1703691, 2018.

[32] S. V. Vassilev and C. G. Vassileva, "Water-soluble fractions of biomass and biomass ash and their significance for biofuel application," *Energy & Fuels*, vol. 33, no. 4, pp. 2763–2777, 2019.

[33] M. Couturier, S. Ladevèze, G. Sulzenbacher et al., "Lytic xylan oxidases from wood-decay fungi unlock biomass degradation," *Nature Chemical Biology*, vol. 14, no. 3, pp. 306–310, 2018.

[34] Y. Rodenas, R. Mariscal, J. L. G. Fierro, D. Martín Alonso, J. A. Dumesic, and M. López Granados, "Improving the production of maleic acid from biomass: TS-1 catalysed aqueous phase oxidation of furfural in the presence of γ-valerolactone," *Green Chemistry*, vol. 20, no. 12, pp. 2845–2856, 2018.

[35] C. R. Correa and A. Kruse, "Supercritical water gasification of biomass for hydrogen production – Review," *The Journal of Supercritical Fluids*, vol. 133, pp. 573–590, 2018.

[36] I. V. Kozhevnikov, "Catalysis by heteropoly acids and multicomponent polyoxometalates in liquid-phase reactions," *Chemical Reviews*, vol. 98, no. 1, pp. 171–198, 1998.

[37] H. Li, H. Wu, H. Zhang, Y. Su, S. Yang, and E. J. M. Hensen, "A facile direct route to N-(un)substituted lactams by cycloamination of oxocarboxylic acids without external hydrogen," *ChemSusChem*, vol. 12, no. 16, pp. 3778–3784, 2019.

[38] Y. Li, L. Shuai, H. Kim et al., "An "ideal lignin" facilitates full biomass utilization," *Science Advances*, vol. 4, no. 9, p. -eaau2968, 2018.

[39] U. Tyagi, N. Anand, and D. Kumar, "Simultaneous pretreatment and hydrolysis of hardwood biomass species catalyzed by combination of modified activated carbon and ionic liquid in biphasic system," *Bioresource Technology*, vol. 289, pp. 121675–121675, 2019.

[40] G. Wen, Q. Gu, Y. Liu et al., "Biomass-derived graphene-like carbon: efficient metal-free carbocatalysts for epoxidation,"

Angewandte Chemie, International Edition, vol. 57, no. 51, pp. 16898–16902, 2018.

[41] R. Fang, P. Tian, X. Yang, R. Luque, and Y. Li, "Encapsulation of ultrafine metal-oxide nanoparticles within mesopores for biomass-derived catalytic applications," *Chemical Science*, vol. 9, no. 7, pp. 1854–1859, 2018.

[42] F. Chacón-Huete, C. Messina, F. Chen, L. Cuccia, X. Ottenwaelder, and P. Forgione, "Solvent-free mechanochemical oxidation and reduction of biomass-derived 5-hydroxymethyl furfural," *Green Chemistry*, vol. 20, no. 23, pp. 5261–5265, 2018.

[43] J. G. Hernández-Cortez, L. Martinez, L. Soto et al., "Liquid phase alkylation of benzene with dec-1-ene catalyzed on supported 12-tungstophosphoric acid," *Catalysis Today*, vol. 150, no. 3-4, pp. 346–352, 2010.

[44] H. Ilbeygi, I. Y. Kim, M. G. Kim et al., "Highly crystalline mesoporous phosphotungstic acid: a high-performance electrode material for energy-storage applications," *Angewandte Chemie, International Edition*, vol. 58, no. 32, pp. 10849–10854, 2019.

[45] P. Meng, H. Heng, Y. Sun, J. Huang, J. Yang, and X. Liu, "Positive effects of phosphotungstic acid on the in-situ solid-state polymerization and visible light photocatalytic activity of polyimide-based photocatalyst," *Applied Catalysis B: Environmental*, vol. 226, pp. 487–498, 2018.

[46] S. K. Bhatia, R. Gurav, T.-R. Choi et al., "Bioconversion of plant biomass hydrolysate into bioplastic (polyhydroxyalkanoates) using _Ralstonia eutropha_ 5119," *Bioresource Technology*, vol. 271, pp. 306–315, 2019.

[47] C. Fang, Y. Li, Z. Yu, H. Li, and S. Yang, "Efficient catalytic upgrade of fructose to alkyl levulinates with phenylpyridine-phosphotungstate solid hybrids," *Current Green Chemistry*, vol. 6, no. 1, pp. 44–52, 2019.

[48] X. Wang, T. Lv, M. Wu et al., "Aluminum doped solid acid with suitable ratio of Brønsted and Lewis acid sites synthesized by electric-flocculation of phosphotungstic acid via hydrothermal treatment for producing 5-hydroxymethylfurfural from glucose," *Appl. Catal. A: Gen.*, vol. 574, pp. 87–96, 2019.

[49] F. Huang, Y. Su, Y. Tao, W. Sun, and W. Wang, "Preparation of 5-hydroxymethylfurfural from glucose catalyzed by silica-supported phosphotungstic acid heterogeneous catalyst," *Fuel*, vol. 226, pp. 417–422, 2018.

[50] Z. Wang, H. Li, C. Fang, W. Zhao, T. Yang, and S. Yang, "Simply assembly of acidic nanospheres for efficient production of 5-ethoxymethylfurfural from 5-hydromethylfurfural and fructose," *Energy Technology*, vol. 5, no. 11, pp. 2046–2054, 2017.

[51] C. Fang, Y. Li, W. Zhao et al., "Phosphotungstic acid heterogenized by assembly with pyridines for efficient catalytic conversion of fructose to methyl levulinate," *RSC Advances*, vol. 8, no. 30, pp. 16585–16592, 2018.

[52] T. CAI, M. YUE, X. WANG, Q. DENG, Z. PENG, and W. ZHOU, "Preparation, characterization, and photocatalytic performance of $NdPW_{12}O_{40}/TiO_2$ composite catalyst," *Chinese Journal of Catalysis*, vol. 28, no. 1, pp. 10–16, 2007.

[53] X. S. Wang, L. Li, J. Liang, Y. B. Huang, and R. Cao, "Boosting oxidative desulfurization of model and real gasoline over phosphotungstic acid encapsulated in metal-organic frameworks: the window size matters," *ChemCatChem*, vol. 9, no. 6, pp. 971–979, 2017.

[54] C. F. Oliveira, L. M. Dezaneti, F. A. C. Garcia et al., "Esterification of oleic acid with ethanol by 12-tungstophosphoric acid supported on zirconia," *Applied Catalysis A: General*, vol. 372, no. 2, pp. 153–161, 2010.

[55] X. Li and Y. Zhang, "The conversion of 5-hydroxymethyl furfural (HMF) to maleic anhydride with vanadium-based heterogeneous catalysts," *Green Chemistry*, vol. 18, no. 3, pp. 643–647, 2016.

[56] T. S. Wang, S. Bao, L. Xu, Z. R. Liu, and L. M. Duan, "The photodegradation performance of phosphotungstic acid/CdS composite materials to organic dyes," *Applied Mechanics and Materials*, vol. 548-549, pp. 25–28, 2014.

[57] S. H. Shinde and C. V. Rode, "An integrated production of diesel fuel precursors from carbohydrates and 2-methylfuran over Sn-mont catalyst," *ChemistrySelect*, vol. 3, no. 15, pp. 4039–4046, 2018.